AIAA 94-3054

Modeling Pyrotechnic Shock in a NASA Standard Initiator Driven Pin Puller

K. A. Gonthier, T. J. Kane, and
J. M. Powers
Department of Aerospace and Mechanical
Engineering
University of Notre Dame
Notre Dame, Indiana

**30th AIAA/ASME/SAE/ASEE Joint
Propulsion Conference
June 27-29, 1994 / Indianapolis, IN**

MODELING PYROTECHNIC SHOCK IN A NASA STANDARD INITIATOR DRIVEN PIN PULLER[*]

Keith A. Gonthier,[†] Thomas J. Kane,[‡] and Joseph M. Powers,[§]
Department of Aerospace and Mechanical Engineering,
University of Notre Dame,
Notre Dame, Indiana 46556-5637.

Abstract

This paper presents an analysis for pyrotechnic combustion and pin motion in the NASA Standard Initiator driven pin puller. The conservation principles and constitutive relations for a multi-phase system are posed and reduced to a set of eight ordinary differential equations which are solved to predict the system performance. The model tracks the interactions of the unreacted, incompressible solid pyrotechnic, incompressible condensed phase combustion products, and gas phase combustion products. The model accounts for multiple pyrotechnic grains, variable burn surface area, combustion product mass flow rates through an orifice located within the device, and pyrotechnic shock. Pressure-time predictions compare favorably with experimental data.

Introduction

Pyrotechnically actuated devices are widely used for aerospace applications. Examples of such devices are pin pullers, exploding bolts, and valves. One such device which has been extensively tested[1] and modeled[2,3] is the NASA Standard Initiator (NSI) driven pin puller. Figure 1 depicts a cross-section of the NSI driven pin puller in its unretracted state. The primary pin, which will be referred to as the pin for the remainder of the paper, is driven by gases generated by the combustion of a pyrotechnic which is contained within the NSI assembly. Two NSI's are tightly threaded into the device's main body. Only one NSI need operate for the proper functioning of the pin puller; the second is a safety precaution in the event of failure of the first. The pyrotechnic consists of a 114 mg mixture of zirconium
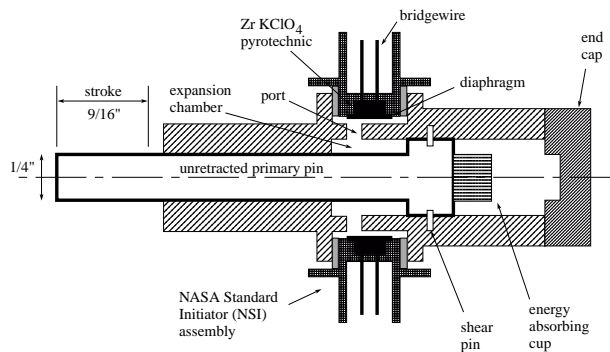
Figure 1: Cross-section of the NSI driven pin puller.

fuel (54.7 mg Zr) and potassium perchlorate oxidizer (59.3 mg $KClO_4$). Initially a thin diaphragm tightly encloses the pyrotechnic. Combustion is initiated by the transfer of heat from an electric bridgewire to the pyrotechnic. Upon ignition, the pyrotechnic undergoes rapid chemical reaction producing both condensed phase and gas phase products. The high pressure products accelerate the combustion rate, burst the confining diaphragm, vent through the NSI port (labeled "port" in Fig. 1), and enter into the gas expansion chamber. Once in the chamber, the high pressure gas first causes a set of shear pins to fail, then pushes the pin. After the pin is stopped by crushing an energy absorbing cup, the operation of the device is complete. Peak pressures within the expansion chamber are typically around 50.0 MPa; completion of the stroke requires approximately 0.5 ms.[1]

The force, commonly referred to as "pyrotechnic shock," often poses a significant hazard in aerospace applications. The recently failed Mars Observer satellite provides an example of how this hazard can have detrimental effects on mission performance[4]. In preparation for the firing of a different device, an NSI-actuated valve, communications transmitters were routinely shut down so as to avoid damage to sensitive filaments in the transmitter tubes due to pyrotechnic shock. In this case the spacecraft never resumed transmission indicating the occurrence of an

accident. Diagnostics proved to be most difficult due to the complete absence of data near the time of failure. Had not the danger of pyrotechnic shock been as severe, it may have been possible to continue data transmission, allowing at a minimum better diagnostics, and possibly even potential failure avoidance.

As a step towards mitigating the hazards of pyrotechnic shock, it is reasonable to first describe the phenomenon. Consequently, the goal of this paper is to characterize pyrotechnic shock in the context of an experimentally verified model which describes the full process of pyrotechnic combustion, pin acceleration and deceleration, and pyrotechnic shock transmission. This paper extends the recent modeling studies of Refs. 2 and 3 to model friction between the piston and wall and the crushing of the end cup. The forces induced by gas pressure, friction, and crushing combine to form the force which is transmitted to the structure: the pyrotechnic shock.

In review of earlier studies, Ref. 2 described a methodology for modeling pyrotechnic combustion driven systems which is based upon principles of mixture theory. This approach offers a framework for 1) accounting for systems in which unreacted solids and condensed phase products form a large fraction of the mass and volume of the total system, and 2) accounting for the transfer of mass, momentum, and energy both within and between phases. The methodology was illustrated by applying it to a device which is well characterized by experiments: the NSI driven pin puller. In Ref. 3, this model was extended to account for 1) choked flow effects of combustion products through the port, and 2) multiple, variable surface area pyrotechnic grains. Additionally, Kuo and Goldstein[5] have taken an alternative approach which utilizes large scale hydrocode modeling of the system response.

Included in this paper are 1) a description of the model composed of the mass, momentum, and energy principles supplemented by geometrical and constitutive relations, 2) the mathematical reductions used to refine the model into a form suitable for numerical computations, and 3) model predictions and comparisons with experimental results.

Model Description

Assumptions for the model are as follows. The total system is taken to consist of four subsystems: incompressible solid pyrotechnic reactants (s), incompressible condensed phase products (cp), gas phase products (g), and the combination of the pin and energy-absorbing cup. The reactants are confined to the NSI assembly, while the products are allowed in both chambers. The reactants are assumed to consist of N spherical grains having uniform instantaneous radii. The surroundings are taken to consist of the walls of the entire assembly, referred to here as the surrounding structure. Both the NSI assembly and the gas expansion chamber are modeled as isothermal cylindrical vessels. The gas expansion chamber is bounded at one end by a mobile, adiabatic pin, while the volume of the NSI assembly remains constant for all time. The port is assumed to have zero volume and is characterized by its cross-sectional area.

Figure 2 depicts the pin and cup moving to the right under the influence of the gas pressure force $F_p(t)$. The motion is being retarded by a wall friction
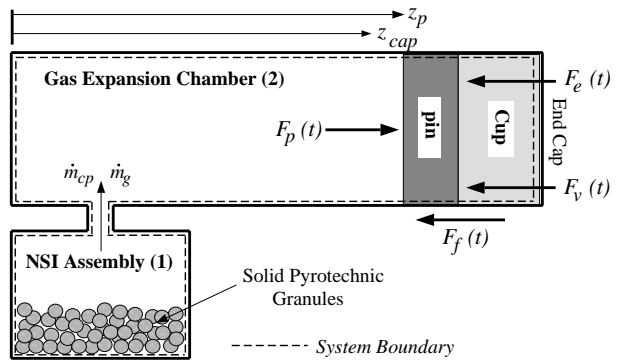

Figure 2: Schematic of the two component system for modeling choked flow effects.

force $F_f(t)$, and elastic and strain-rate dependent cup deformation forces $F_e(t)$ and $F_v(t)$, respectively. The model is constructed such that deformation forces are triggered when the instantaneous pin position z_p is greater than a constant z_{cap}. When $z_p = z_{cap}$, the pin and cup combination comes into contact with the end cap. In contrast to Fig. 1, Fig. 2 depicts the pin and cup combination in a position in which the cup is being deformed.

Mass and heat exchange between subsystems is allowed such that 1) mass can be transferred from the solid pyrotechnic to both the condensed phase and gas phase products, and 2) heat can be transferred from the condensed phase to the gas phase products. The condensed phase - gas phase heat transfer rate is assumed to be sufficiently large such that thermal equilibrium between the product subsystems exists. There is no mass exchange between the system and the surroundings. Both product subsystems are allowed to interact across the system boundary in the form of heat exchanges. The gas phase products are allowed to do expansion work on the pin. Due to friction and cup crushing, the pin exchanges work with the surroundings. Spatial variations within sub-

2

systems are neglected; consequently, all variables are only time-dependent, and the total system is modeled as a well-stirred reactor. The kinetic energy of the reactants, condensed product, and gas product subsystems is ignored, while an accounting is made of the kinetic energy of the pin.

The rate of mass exchange from the reactant subsystem to the product subsystems is taken to be related to the gas phase pressure within the NSI assembly, namely $dr/dt = -bP_{g_1}^n$, where r is the instantaneous radii of the pyrotechnic grains, t is time, P_{g_1} is the gas phase pressure within the NSI assembly, and b and n are experimentally determined constants. All combustion is restricted to the burn surface of the pyrotechnic grains. We have chosen values for b and n so that some limited available strand burning data for $ZrKClO_4$ can be matched. We hypothesize that the bridgewire initiation breaks the pyrotechnic into a large number of particles and estimate the number of particles so that experimentally determined pressure-time traces can be matched. The equilibrium thermochemistry code CET89[6], used here to model the constant volume complete combustion of the $Zr/KClO_4$ mixture, predicts the product composition. The initial total volume of the pin puller ($0.95\ cm^3$) was used in this calculation since a significant portion of the system mass is contained within the gas expansion chamber at the time of complete combustion. The component gases are taken to be ideal with temperature-dependent specific heats. The specific heats are in the form of fourth-order polynomial curve fits given by the CET89 code and are not repeated.

The rate of gas phase product mass flowing from the NSI assembly, through the port, and into the gas expansion chamber is modeled using standard principles of gas dynamics. The flow of condensed phase product mass through the port is assumed to be proportional to the gas phase mass flow rate. The only energy interaction between the NSI assembly and the gas expansion chamber is due to the convective energy flux between these two components.

Using principles of mixture theory, a set of mass and energy evolution equations can be written for solid pyrotechnic, condensed phase, and gas phase subsystems. These equations, coupled with an equation of motion for the pin, form a set of ordinary differential equations (ODE's) given by the following:

$$\frac{d}{dt}\left(\rho_{s_1} V_{s_1}\right) = -\rho_{s_1} A_b r_b, \qquad (1)$$

$$\frac{d}{dt}\left(\rho_{cp_1} V_{cp_1}\right) = \eta_{cp}\rho_{s_1} A_b r_b - \dot{m}_{cp}, \qquad (2)$$

$$\frac{d}{dt}\left(\rho_{g_1} V_{g_1}\right) = \left(1 - \eta_{cp}\right)\rho_{s_1} A_b r_b - \dot{m}_g, \qquad (3)$$

$$\frac{d}{dt}\left(\rho_{s_1} V_{s_1} e_{s_1}\right) = -\rho_{s_1} e_{s_1} A_b r_b, \qquad (4)$$

$$\frac{d}{dt}\left(\rho_{cp_1} V_{cp_1} e_{cp_1}\right)$$
$$= \eta_{cp}\rho_{s_1} e_{s_1} A_b r_b - h_{cp_1}\dot{m}_{cp} - \dot{Q}_{cp,g_1} + \dot{Q}_{cp_1}, \qquad (5)$$

$$\frac{d}{dt}\left(\rho_{g_1} V_{g_1} e_{g_1}\right)$$
$$= \left(1 - \eta_{cp}\right)\rho_{s_1} e_{s_1} A_b r_b - h_{g_1}\dot{m}_g + \dot{Q}_{cp,g_1} + \dot{Q}_{g_1}, \qquad (6)$$

$$\frac{d}{dt}\left(\rho_{cp_2} V_{cp_2}\right) = \dot{m}_{cp}, \qquad (7)$$

$$\frac{d}{dt}\left(\rho_{g_2} V_{g_2}\right) = \dot{m}_g, \qquad (8)$$

$$\frac{d}{dt}\left(\rho_{cp_2} V_{cp_2} e_{cp_2}\right) = h_{cp_1}\dot{m}_{cp} - \dot{Q}_{cp,g_2} + \dot{Q}_{cp_2}, \qquad (9)$$

$$\frac{d}{dt}\left(\rho_{g_2} V_{g_2} e_{g_2}\right) = h_{g_1}\dot{m}_g + \dot{Q}_{cp,g_2} + \dot{Q}_{g_2} - \dot{W}_{out_2}, \qquad (10)$$

$$m_p\frac{d^2}{dt^2}\left(z_p\right) = F_p - F_f - F_e - F_v. \qquad (11)$$

In these equations, the subscripts "1" and "2" are used to label quantities associated with the NSI and the gas expansion chamber, respectively. Subscripts "s", "cp", and "g" are used to label quantities associated with the solid pyrotechnic, condensed phase products, and gas phase products, respectively. The independent variable in Eqs. (1-11) is time t. Dependent variables are as follows: the density ρ_{g_i} (here, and for the remainder of this report, the index $i = 1, 2$ will be used to denote quantities associated with the NSI and the gas expansion chamber, respectively); the volumes V_{s_1}, V_{cp_i}, V_{g_i}; the specific internal energies e_{s_1}, e_{cp_i}, e_{g_i}; the specific enthalpies h_{cp_1}, h_{g_1}; the pin position z_p; the pyrotechnic burn rate r_b; the area of the burn surface A_b; the rates of product mass flowing through the port $\dot{m}_{cp}$, $\dot{m}_g$; the rates of heat transfer from the surroundings to the gas phase products $\dot{Q}_{in_i}$; the rates of heat transfer from the condensed phase products to the gas phase products $\dot{Q}_{cp,g_i}$; the rate of work done by product gases contained within the expansion chamber in moving the pin $\dot{W}_{out_2}$; and the force on the pin due to gas pressure, wall friction, elastic cup deformation, and velocity-dependent cup deformation, F_p, F_f, F_e, F_v, respectively.

Constant parameters contained in Eqs. (1-11) are the mass of the pin m_p, the density of the unreacted solid pyrotechnic ρ_{s_1}, the density of the condensed phase products ρ_{cp_1} and ρ_{cp_2}, and the mass fraction of the products which are in the condensed phase η_{cp}. As it is understood that the pyrotechnic is

contained entirely within the NSI, the notation subscript "1" will be dropped when referring to quantities associated with the solid pyrotechnic. Also, since $\rho_{cp_1} = \rho_{cp_2} =$ constant, these two quantities will be referred to as ρ_{cp}.

Equations (1-3) govern the evolution of mass, and Eqs. (4-6) govern the evolution of energy for the solid pyrotechnic, the condensed phase products, and the gas phase products contained within the NSI, respectively. Equations (7) and (8) govern the evolution of mass, and Eqs. (9) and (10) govern the evolution of energy for the condensed phase products and gas phase products contained within the gas expansion chamber, respectively. Equation (11) is Newton's Second Law which governs the motion of the pin.

Geometric and constitutive relations used to close Eqs. (1-11) are as follows:

$$V_1 = V_s + V_{cp_1} + V_{g_1}, \tag{12}$$

$$V_2 = V_{cp_2} + V_{g_2}, \tag{13}$$

$$z_p = \frac{V_2}{A_p}, \tag{14}$$

$$r\,[V_s] = \left(\frac{3V_s}{4\pi N}\right)^{1/3}, \tag{15}$$

$$A_b\,[V_s] = \left(36\pi N V_s^2\right)^{1/3}, \tag{16}$$

$$P_{g_i} = \rho_{g_i} R T_{g_i}, \tag{17}$$

$$r_b\,[P_{g_1}] = -\frac{dr}{dt} = b P_{g_1}^n, \tag{18}$$

$$e_s\,[T_s] = \sum_{j=1}^{N_s} Y_s^j e_s^j\,[T_s], \tag{19}$$

$$e_{cp_i}\,[T_{cp_i}] = \sum_{j=1}^{N_{cp}} Y_{cp}^j e_{cp}^j\,[T_{cp_i}], \tag{20}$$

$$e_{g_i}\,[T_{g_i}] = \sum_{j=1}^{N_g} Y_g^j e_g^j\,[T_{g_i}], \tag{21}$$

$$c_{vs}\,[T_s] = \sum_{j=1}^{N_s} Y_s^j \frac{d}{dT_s}\left(e_s^j\,[T_s]\right), \tag{22}$$

$$c_{vcp_i}\,[T_{cp_i}] = \sum_{j=1}^{N_{cp}} Y_{cp}^j \frac{d}{dT_{cp_i}}\left(e_{cp}^j\,[T_{cp_i}]\right), \tag{23}$$

$$c_{vg_i}\,[T_{g_i}] = \sum_{j=1}^{N_g} Y_g^j \frac{d}{dT_{g_i}}\left(e_g^j\,[T_{g_i}]\right), \tag{24}$$

$$h_{cp_1}\,[T_{cp_1}] = \sum_{j=1}^{N_{cp}} Y_{cp}^j h_{cp}^j\,[T_{cp_1}], \tag{25}$$

$$h_{g_1}\,[T_{g_1}] = \sum_{j=1}^{N_g} Y_g^j h_g^j\,[T_{g_1}], \tag{26}$$

$$c_{pcp_1}\,[T_{cp_1}] = \sum_{j=1}^{N_{cp}} Y_{cp}^j \frac{d}{dT_{cp_1}}\left(h_{cp}^j\,[T_{cp_1}]\right), \tag{27}$$

$$c_{pg_1}\,[T_{g_1}] = \sum_{j=1}^{N_g} Y_g^j \frac{d}{dT_{g_1}}\left(h_g^j\,[T_{g_1}]\right), \tag{28}$$

$$\dot{Q}_{cp,g_i}\,[T_{cp_i}, T_{g_i}] = h_{cp,g} A_{cp_i}\left(T_{cp_i} - T_{g_i}\right), \tag{29}$$

$$\dot{Q}_{cp_i} = \dot{Q}_{cp_i}\,[T_{cp_i}], \tag{30}$$

$$\dot{Q}_{g_i} = \dot{Q}_{g_i}\,[T_{g_i}], \tag{31}$$

$$\dot{W}_{out_2} = P_{g_2}\frac{dV_2}{dt}, \tag{32}$$

$$F_p = \begin{cases} 0 & \text{if } P_{g_2} A_p < F_{crit} \\ P_{g_2} A_p & \text{if } P_{g_2} A_p \geq F_{crit}, \end{cases} \tag{33}$$

$$F_f = C_f\frac{dz_p}{dt} \tag{34}$$

$$F_e = \begin{cases} 0 & \text{if } z_p < z_{cap} \\ C_e(z_p - z_{cap}) & \text{if } z_p \geq z_{cap}, \end{cases} \tag{35}$$

$$F_v = \begin{cases} 0 & \text{if } z_p < z_{cap} \\ C_v\frac{dz_p}{dt} & \text{if } z_p \geq z_{cap}, \end{cases} \tag{36}$$

$$F_{ps} = -F_p + F_f + F_e + F_v \tag{37}$$

$$\dot{m}_g = \begin{cases} \rho_{g_1} A_e \sqrt{\gamma R T_{g_1}} \\ \quad \times \sqrt{\frac{2}{\gamma-1}\left(\frac{P_{g_1}}{P_{g_2}}\right)^{-\frac{\gamma+1}{\gamma}}\left(\left(\frac{P_{g_1}}{P_{g_2}}\right)^{\frac{\gamma-1}{\gamma}} - 1\right)} \\ \quad \text{if } \left(\frac{P_{g_1}}{P_{g_2}}\right) < \left(\frac{\gamma+1}{2}\right)^{\frac{\gamma}{\gamma-1}}, \\ \rho_{g_1} A_e \sqrt{\gamma R T_{g_1}}\left(\frac{2}{\gamma+1}\right)^{\frac{\gamma+1}{2(\gamma-1)}} \\ \quad \text{if } \left(\frac{P_{g_1}}{P_{g_2}}\right) \geq \left(\frac{\gamma+1}{2}\right)^{\frac{\gamma}{\gamma-1}}, \end{cases} \tag{38}$$

$$\dot{m}_{cp} = \left(\frac{\eta_{cp}}{1 - \eta_{cp}}\right)\dot{m}_g. \tag{39}$$

Here, and throughout the paper, braces [ ] are used to denote a functional dependence on the enclosed variable. Equations (12-14) are geometrical constraints; in Eq. (14), A_p is the cross-sectional area of the pin. Equation (15) is an expression for the radius r of each spherical pyrotechnic grain; N is the total number of pyrotechnic grains. The area of the burn surface is given by Eq. (16); it is assumed here that the area of the burning surface is the total surface area of the N pyrotechnic grains. Equation (17) is a thermal equation of state for the gas phase products. Occurring in this expression are the gas phase pressure P_{g_i}, the gas phase temperature T_{g_i}, and the ideal gas constant

for the gas phase products R (the quotient of the universal gas constant and the mean molecular weight of the product gases). The pyrotechnic burn rate r_b is given by Eq. (18).

Equations (19-21) are caloric equations of state for the solid pyrotechnic, condensed phase products, and gas phase products, respectively. Here, T_s is the temperature of the solid pyrotechnic, and T_{cp_i} is the temperature of the condensed phase products. Also, Y_s^j, $Y_{cp_i}^j$, $Y_{g_i}^j$, N_s, N_{cp}, and N_g are the constant mass fractions and number of component species of solid pyrotechnic, condensed phase product, and gas phase product species, respectively. Here, and throughout the paper, the notation superscript "j" is used to label quantities associated with individual chemical species. Since for both ideal gases and condensed phase species, the internal energy is only a function of temperature, the specific heat at constant volume for the solid pyrotechnic, c_{vs}, the condensed phase products, c_{vcp_i}, and the gas phase products, c_{vg_i}, can be obtained by differentiation of Eqs. (19-21) with respect to their temperature. Expressions for the specific heats at constant volume are given by Eqs. (22-24). The specific enthalpies for the condensed phase products and the gas phase products contained within the NSI assembly are given by Eqs. (25) and (26), respectively. These expressions can be differentiated with respect to their temperature to obtain the specific heats at constant pressure c_{pcp_1} and c_{pg_1}, Eqs. (27) and (28).

Equation (29) gives an expression for the rate of heat transfer from the condensed phase products to the gas phase products. In this expression, $h_{cp,g}$ is a constant heat transfer parameter, and A_{cp_i} is the surface area of the condensed phase products. The term $h_{cp,g}A_{cp_i}$ is assumed large for this study. The functional dependencies of the heat transfer rates between the surroundings and the product subsystems are given by Eqs. (30) and (31). The functional form of these models will be given below.

Equation (32) models pressure-volume work done by the gas contained within the expansion chamber in moving the pin. Equation (33) models the force on the pin due to the gas phase pressure and a restraining force due to the shear pins which are used to initially hold the pin in place. Here, F_{crit} is the critical force necessary to cause shear pin failure. The work associated with shearing the pin is not considered. Equation (34) models the wall friction force as proportional by a constant factor C_f to the piston velocity. When the pin motion places the cup in contact with the end cap, at $z_p = z_{cap}$, additional forces are modeled. The elastic force is modeled in Eq. (35) as proportional by a factor C_e to the displacement

$(z_p - z_{cap})$, and a velocity (strain-rate) dependent force is modeled in Eq. (36) as proportional by a factor C_v to the pin velocity. Equation (37) gives the pyrotechnic shock force, F_{ps}, defined positive when pointing to the left. Effectively, F_{ps} represents the external force necessary to hold the surrounding structure stationary during the stroking of the pin. With this sign convention, positive friction and deformation forces give the surrounding structure a tendency to move to the right; to balance these, a positive F_{ps} is required. A positive pressure force, while pushing the pin to the right, will push against the wall opposite to the pin, tending to move the surrounding structure to the left, thus requiring a rightward facing (negative) F_{ps} to maintain static equilibrium.

The flow rate of gas phase product mass through the port is given by Eq. (38).[7] Occurring in this expression are the cross-sectional area of the port, A_e, and the specific heat ratio for the product gases contained within the NSI assembly, $\gamma \ (= c_{pg_1}/c_{vg_1})$. This expression accounts for mass choking at elevated NSI assembly/gas expansion chamber pressure ratios. The condensed phase product mass flow rate through the port given Eq. (39) guarantees that the mass fraction of the condensed phase products remains the same in both chambers.

With the assumption of large heat transfer rates between the condensed phase and gas phase product subsystems (i.e., $h_{cp,g}A_{cp_i} \rightarrow \infty$), the product subsystems remain in thermal equilibrium for all time. Therefore, we take $T_{p_1} \equiv T_{cp_1} = T_{g_1}$ and $T_{p_2} \equiv T_{cp_2} = T_{g_2}$, with T_{p_1} defined as the temperature of the combined product subsystem contained within the NSI assembly and T_{p_2} the temperature of the combined product subsystem contained within the gas expansion chamber. With this assumption, one can define the net heat transfer rates $\dot{Q}_{p_1}$ and $\dot{Q}_{p_2}$ governing the transfer of heat from the surroundings to the combined product subsystems:

$$\dot{Q}_{p_1}[T_{p_1}] \equiv \dot{Q}_{cp_1} + \dot{Q}_{g_1}$$
$$= hA_{w_1}(T_w - T_{p_1}) + \sigma A_{w_1}(\alpha T_w^4 - \epsilon T_{p_1}^4), \tag{40}$$

$$\dot{Q}_{p_2}[T_{p_2}] \equiv \dot{Q}_{cp_2} + \dot{Q}_{g_2}$$
$$= hA_{w_2}[V_s](T_w - T_{p_2}) + \sigma A_{w_2}[V_2](\alpha T_w^4 - \epsilon T_{p_2}^4), \tag{41}$$

where

$$A_{w_1} = 2\sqrt{\frac{\pi}{A_1}}V_1 + 2A_1 - A_e, \tag{42}$$

$$A_{w_2}[V_2] = 2\sqrt{\frac{\pi}{A_p}}V_2 + A_p - A_e. \tag{43}$$

Equations (42, 43) are expressions for the surface area of the NSI assembly and the gas expansion chamber, respectively, through which heat transfer with the surroundings can occur; the parameter A_1 in the first of these relations is the constant cross-sectional area of the NSI assembly.

Mathematical Reductions

In this section, intermediate operations are described that reduce the governing equations to a final autonomous system of first order ODE's which can be numerically solved to predict the pin puller performance. To this end, it is necessary to define a new variable $\dot{V}_2$ representing the time derivative of the gas expansion chamber volume:

$$\dot{V}_2 \equiv \frac{dV_2}{dt}. \qquad (44)$$

The final system consists of eight first order ODE's of the form

$$\frac{d\mathbf{u}}{dt} = \mathbf{f}(\mathbf{u}), \qquad (45)$$

where $\mathbf{u} = (V_2, V_s, V_{cp_1}, \rho_{g_1}, T_{p_1}, V_{cp_2}, T_{p_2}, \dot{V}_2)^T$ is a vector of dependent variables and $\mathbf{f}$ is a non-linear vector function. These eight dependent variables will be referred to as primary variables. It will now be shown how to express all remaining variables as functions of the primary variables.

Quantities already expressed in terms of the primary variables are the gas phase pressure inside the NSI $P_{g_1}[\rho_{g_1}, T_{p_1}]$, the heat transfer rates $\dot{Q}_{p_1}[T_{p_1}]$ and $\dot{Q}_{p_2}[V_2, T_{p_2}]$, the specific internal energies $e_{cp_i}[T_{p_i}]$ and $e_{g_i}[T_{p_i}]$, the specific heats at constant volume $c_{vcp_i}[T_{p_i}]$ and $c_{vg_i}[T_{p_i}]$, the specific enthalpies $h_{cp_1}[T_{p_1}]$ and $h_{g_1}[T_{p_1}]$, and the specific heats at constant pressure $c_{pcp_1}[T_{p_1}]$ and $c_{pg_1}[T_{p_1}]$.

With a knowledge of P_{g_1}, Eq. (18) can be used to express r_b as functions of ρ_{g_1} and T_{p_1}:

$$r_b[\rho_{g_1}, T_{p_1}] = bP_{g_1}^n[\rho_{g_1}, T_{p_1}]. \qquad (46)$$

Addition of Eqs. (1), (2), (3), (7), and (8) results in a homogeneous differential equation expressing the conservation of the total reactant and product mass:

$$\frac{d}{dt}\left(\rho_s V_s + \rho_{cp} V_{cp_1} + \rho_{g_1} V_{g_1} + \rho_{cp} V_{cp_2} + \rho_{g_2} V_{g_2}\right) = 0. \qquad (47)$$

Integrating this expression, applying initial conditions, denoted by the subscript "o", using Eq. (12) to eliminate V_{g_1} in favor of V_1, V_s, and V_{cp_1}, using Eq. (13) to eliminate V_{g_2} in favor of V_2 and V_{cp_2}, and

solving for ρ_{g_2} results in the following:

$$\rho_{g_2}[V_2, V_s, V_{cp_1}, \rho_{g_1}, V_{cp_2}]$$

$$= [m_o - \rho_s V_s - \rho_{cp} V_{cp_1} - \rho_{g_1}(V_1 - V_s - V_{cp_1})$$

$$- \rho_{cp} V_{cp_2}] \div [V_2 - V_{cp_2}], \qquad (48)$$

where

$$m_o = \rho_s V_{s_o} + \rho_{cp} V_{cp_1 o} + \rho_{g_1} V_{g_1 o} + \rho_{cp} V_{cp_2 o} + \rho_{g_2} V_{g_2 o}.$$

Here, m_o represents the initial mass of the system.

Substituting Eq. (48) into Eq. (17) determines P_{g_2} as a function of the primary variables:

$$P_{g_2}[V_2, V_s, V_{cp_1}, \rho_{g_1}, V_{cp_2}, T_{p_2}]$$

$$= \rho_{g_2}[V_2, V_s, V_{cp_1}, \rho_{g_1}, V_{cp_2}] R T_{p_2}. \qquad (49)$$

With a knowledge of P_{g_2}, Eqs. (32), (33), (38), and (39) can be expressed in the following forms, respectively:

$$\dot{W}_{out2} = \dot{W}_{out2}[V_2, V_s, V_{cp_1}, \rho_{g_1}, V_{cp_2}, T_{p_2}, \dot{V}_2], \quad (50)$$

$$F_p = F_p[V_2, V_s, V_{cp_1}, \rho_{g_1}, V_{cp_2}, T_{p_2}], \qquad (51)$$

$$\dot{m}_g = \dot{m}_g[V_2, V_s, V_{cp_1}, \rho_{g_1}, T_{p_1}, V_{cp_2}, T_{p_2}], \qquad (52)$$

$$\dot{m}_{cp} = \dot{m}_{cp}[V_2, V_s, V_{cp_1}, \rho_{g_1}, T_{p_1}, V_{cp_2}, T_{p_2}]. \qquad (53)$$

With Eqs. (14), (44), and (51), the equations (34-37) for the various forces can be written as follows:

$$F_f[\dot{V}_2] = \frac{C_f}{A_p}\dot{V}_2, \qquad (54)$$

$$F_e[V_2] = \frac{C_e}{A_p}(V_2 - z_{cap} A_p), \qquad (55)$$

$$F_v[\dot{V}_2] = \frac{C_v}{A_p}\dot{V}_2, \qquad (56)$$

$$F_{ps} = F_{ps}\left[V_2, V_s, V_{cp_1}, \rho_{g_1}, V_{cp_2}, T_{p_2}, \dot{V}_2\right]. \qquad (57)$$

We next simplify the remaining mass evolution equations. Since both ρ_s and ρ_{cp} are constant, Eqs. (1), (2), and (7) can be rewritten as

$$\frac{dV_s}{dt} = -A_b r_b, \qquad (58)$$

$$\frac{dV_{cp_1}}{dt} = \frac{\eta_{cp}\rho_s A_b r_b - \dot{m}_{cp}}{\rho_{cp}}, \qquad (59)$$

$$\frac{dV_{cp_2}}{dt} = \frac{\dot{m}_{cp}}{\rho_{cp}}. \qquad (60)$$

To simplify Eq. (3), we use Eq. (12) to replace V_{g_1} in favor of V_s and V_{cp_1}, use Eqs. (58) and (59) to

eliminate the resulting volume derivatives, and solve for the time derivative of ρ_{g_1}:

$$\frac{d\rho_{g_1}}{dt} = [(1 - \rho_{g_1}/\rho_s - (1 - \rho_{g_1}/\rho_{cp})\,\eta_{cp})\,\rho_s A_b r_b$$

$$-\dot{m}_g - \dot{m}_{cp}\rho_{g_1}/\rho_{cp}] \div [V_1 - V_s - V_{cp_1}]. \qquad (61)$$

The energy evolution equations will now be simplified. We first multiply Eq. (1) by e_s and subtract the result from Eq. (4) to obtain

$$\frac{de_s}{dt} = 0.$$

Thus the reactants' specific internal energy remains constant for all time. Integrating this result, we obtain

$$e_s = e_{so}. \qquad (62)$$

Addition of Eqs. (5) and (6), and addition of Eqs. (9) and (10) result in expressions governing the evolution of energy for the combined product subsystems contained within the NSI assembly and gas expansion chamber, respectively:

$$\frac{d}{dt}\left[\rho_{cp}V_{cp_1}e_{cp_1} + \rho_{g_1}V_{g_1}e_{g_1}\right]$$

$$= \rho_s e_s A_b r_b - h_{cp_1}\dot{m}_{cp} - h_{g_1}\dot{m}_g + \dot{Q}_{p_1}, \qquad (63)$$

$$\frac{d}{dt}\left[\rho_{cp}V_{cp_2}e_{cp_2} + \rho_{g_2}V_{g_2}e_{g_2}\right]$$

$$= h_{cp_1}\dot{m}_{cp} + h_{g_1}\dot{m}_g + \dot{Q}_{p_2} - \dot{W}_{out_2}. \qquad (64)$$

The net heat transfer rates given by Eqs. (40) and (41) have been incorporated into these expressions. Multiplying Eq. (2) by e_{cp_1}, multiplying Eq. (3) by e_{g_1}, subtracting these results from Eq. (63), using Eqs. (20) and (21) to rewrite the derivatives in terms of T_{p_1}, and solving for dT_{p_1}/dt yields:

$$\frac{dT_{p_1}}{dt} = [\rho_s\,(e_s - \eta_{cp}e_{cp_1} - (1 - \eta_{cp})\,e_{g_1})\,A_b r_b$$

$$- (h_{cp_1} - e_{cp_1})\,\dot{m}_{cp} - (h_{g_1} - e_{g_1})\,\dot{m}_g + \dot{Q}_{p_1}]$$

$$\div [\rho_{cp}V_{cp_1}c_{vcp_1} + \rho_{g_1}V_{g_1}c_{vg_1}]. \qquad (65)$$

Similarly, multiplying Eq. (7) by e_{cp_2}, multiplying Eq. (8) by e_{g_2}, subtracting these results from Eq. (64), using Eqs. (20) and (21) to rewrite the derivatives in terms of T_{p_2}, and solving for dT_{p_2}/dt yields:

$$\frac{dT_{p_2}}{dt} = \left[(h_{cp_1} - e_{cp_2})\,\dot{m}_{cp} + (h_{g_1} - e_{g_2})\,\dot{m}_g + \dot{Q}_{p_2}\right.$$

$$\left. - \dot{W}_{out_2}\right] \div [\rho_{cp}V_{cp_2}e_{cp_2}c_{vcp_2} + \rho_{g_2}V_{g_2}c_{vg_2}]. \qquad (66)$$

Lastly, Eq. (11) can be split into two first order ODE's. The first of these equations is given by the definition presented in Eq. (44). The second equation, obtained by using Eq. (44) and the geometrical relation given by Eq. (14), is expressed by the following:

$$\frac{d\dot{V}_2}{dt} = \frac{A_p}{m_p}\,(F_p - F_f - F_e - F_v). \qquad (67)$$

Equation (44), (58), (59), (61), (65), (60), (66), and (67) form a coupled set of eight non-linear first order ODE's in eight unknowns. Initial conditions for these equations are

$$
\begin{aligned}
&V_2(t=0) = V_{2o}, &\qquad &V_s(t=0) = V_{so}, \\
&V_{cp_1}(t=0) = V_{cp_1 o}, &\qquad &\rho_{g_1}(t=0) = \rho_{g_1 o}, \\
&T_{p_1}(t=0) = T_o, &\qquad &V_{cp_2}(t=0) = V_{cp_2 o}, \\
&T_{p_2}(t=0) = T_o, &\qquad &\dot{V}_2(t=0) = 0.
\end{aligned}
$$
$$(68)$$

All other quantities of interest can be obtained once this system of differential equations is solved.

Results

Numerical solutions were obtained for the simulated firing of an NSI into the pin puller device. The numerical algorithm used to perform the integrations was a stiff ODE solver given in the standard code LSODE. The combustion process predicted by the CET89 chemical equilibrium code followed the reaction equation given in Table 1. Parameters used in the simulations are given in Table 2.

Parametric values for C_e and C_v were chosen so that Bement's[1] energy-absorbing cup impact data could be matched. In these tests, a mass was dropped onto the system, and the final cup deflection was measured as a function of the dropped mass's kinetic energy at the time of impact. It is seen from Fig. 3, which gives results of a simulation of Bement's test, that the values chosen for C_e and C_v allow a approximate match of the data.

Predictions for the pressure history inside the NSI and the gas expansion chamber are shown in Fig. 4. Also shown are experimental values obtained by a pressure transducer threaded into the pinpuller in place of the redundant NSI.[8] The burn rate parameters b and n match the independently predicted strand burning data of Baglini.[9] The number of particles N is then selected specifically so that pressure predictions agree with measurements. A rapid increase in pressure is predicted within the NSI assembly following combustion initiation ($t = 0$ ms); the pressure rises to a maximum value near 225 MPa occurring near the time of complete combustion ($t = 0.028$ ms). The pressure within the expansion
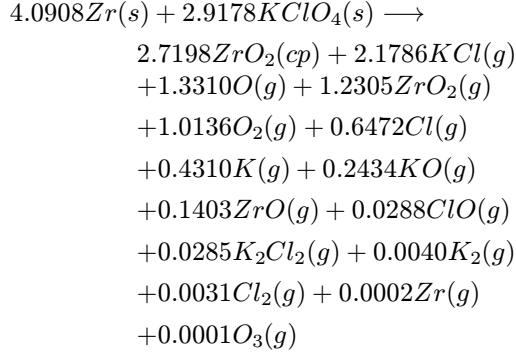
Table 1: Reaction equation.

$$4.0908 Zr(s) + 2.9178 KClO_4(s) \longrightarrow$$
$$2.7198 ZrO_2(cp) + 2.1786 KCl(g)$$
$$+1.3310 O(g) + 1.2305 ZrO_2(g)$$
$$+1.0136 O_2(g) + 0.6472 Cl(g)$$
$$+0.4310 K(g) + 0.2434 KO(g)$$
$$+0.1403 ZrO(g) + 0.0288 ClO(g)$$
$$+0.0285 K_2Cl_2(g) + 0.0040 K_2(g)$$
$$+0.0031 Cl_2(g) + 0.0002 Zr(g)$$
$$+0.0001 O_3(g)$$

Table 2: Parameters used in pin puller simulation.

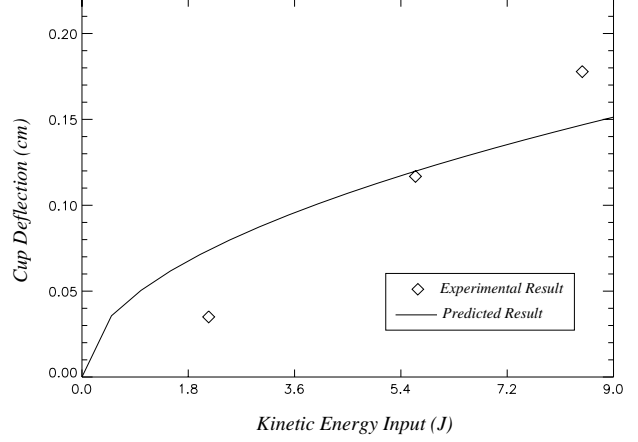| parameter	value
A_1	$0.634\ cm^2$
A_e	$0.100\ cm^2$
A_p	$0.634\ cm^2$
b	$3.0 \times 10^{-6}\ (dyne/cm^2)^{-0.79} cm/s$
C_e	$2.344 \times 10^9\ dyne/cm$
C_f	$7.925 \times 10^4\ dyne\ s/cm$
C_v	$1.37 \times 10^5\ dyne\ s/cm$
F_{crit}	$3.56 \times 10^7\ dyne$
h	$1.25 \times 10^6\ g/s^3/K$
m_p	$19.0\ g$
n	0.79
N	1.0×10^6
T_o	$288.0\ K$
T_w	$288.0\ K$
V_1	$0.125\ cm^3$
V_{2o}	$0.824\ cm^3$
$V_{cp_1 o}$	$7.425 \times 10^{-8}\ cm^3$
$V_{cp_2 o}$	$6.576 \times 10^{-7}\ cm^3$
V_{so}	$0.038\ cm^3$
$\dot{V}_2$	$0.0\ cm^3/s$
z_{cap}	$2.222\ cm$
α	0.60
ϵ	0.60
η_{cp}	0.43
ρ_{cp}	$5.89\ g/cm^3$
$\rho_{g_1 o}$	$6.202 \times 10^{-6}\ g/cm^3$
ρ_s	$3.57\ g/cm^3$

Figure 3: Predicted and measured cup deflection for varying pin kinetic energy of impact.
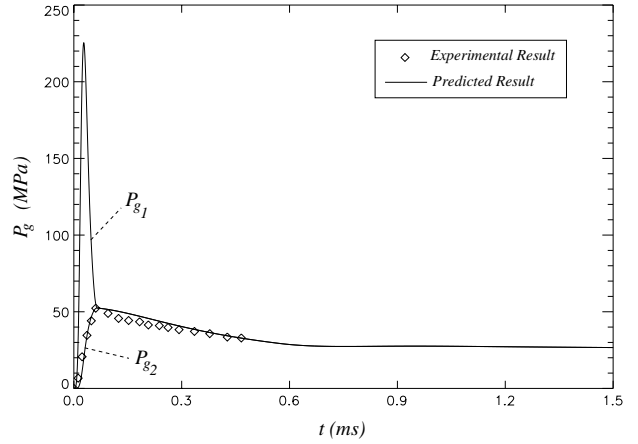

Figure 4: Predicted and measured pressure.

chamber increases more slowly due to choking at the port. Following completion of the combustion process, the pressure within the NSI assembly decreases to near $52\ MPa$ occurring near $t = .065\ ms$; during this same time, the pressure within the gas expansion chamber uniformly increases to near $52\ MPa$. There is a subsequent decrease in both pressures to values near $26\ MPa$ at completion of the pin's stroke ($t_{st} = 0.57\ ms$). These decreases result from work done by the product gases in moving the pin and heat transfer from the combined product subsystems to the surroundings. Here the heat transfer and wall friction coefficients have been chosen so as to allow a close match of the data.

Predictions for the product temperatures within the NSI and the gas expansion chamber are shown in Fig. 5. Temperatures in both components rapidly rise to over $5,000\ K$ and then decrease due to expansion and heat transfer to the surroundings. Since the only
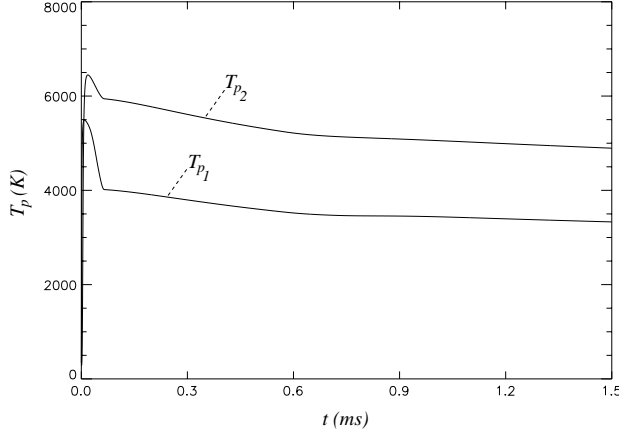
8

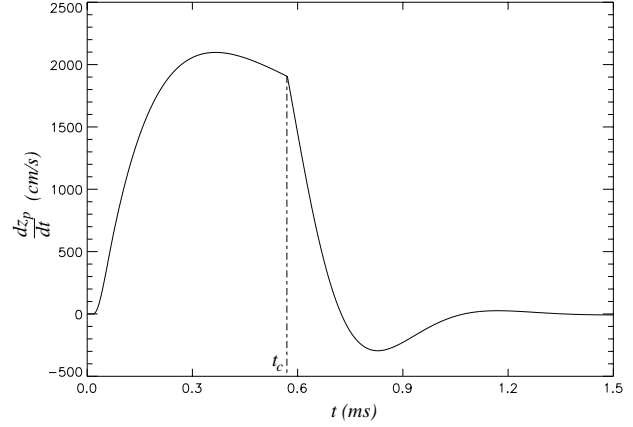Figure 5: Predicted temperature histories.

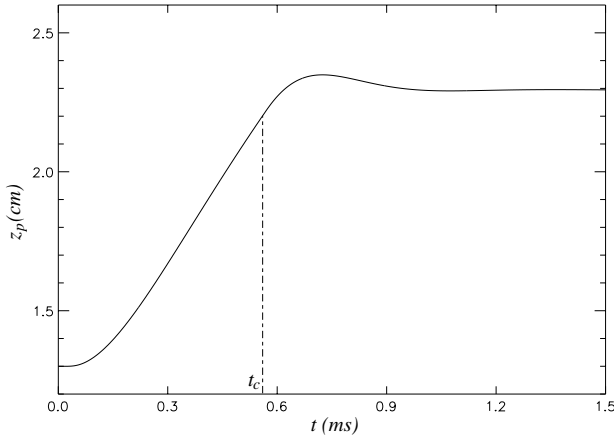Figure 7: Pin velocity vs. time.

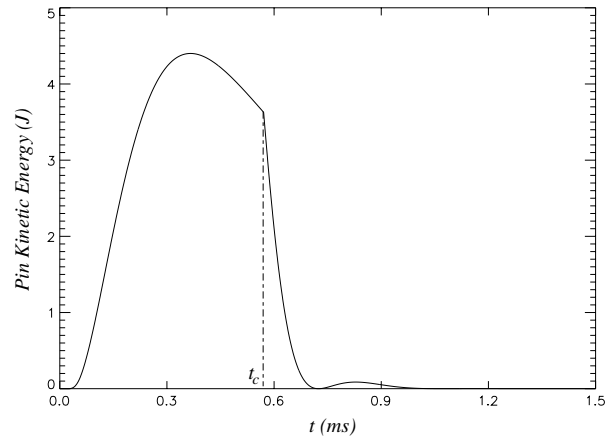
Figure 6: Pin position vs. time.

Figure 8: Pin kinetic energy vs. time.

modeled mechanism of temperature equilibration between subsystems is the relatively slow heat transfer from subsystems to surroundings, the resulting temperatures of the combined product subsystems do not equilibrate within the examined time scales.

Figures 6 and 7 show the position and velocity, respectively, of the pin as functions of time. In these figures, t_c marks the time at which the cup initially impacts the end cap ($0.57\ ms$). It is seen from Fig. 6 that the pin overshoots the value of z_{cap} by $0.113\ cm$, and then relaxes to a position of $2.29\ cm$. The velocity of the pin is initially predicted to increase to a maximum value of $2,097\ cm/s$ (at $t = 0.37\ ms$) and then to smoothly decrease to near $1,900\ cm/s$ at the time of impact of the cup with the end cap. Upon impact, the velocity of the pin rapidly decreases and approaches zero as the pin is stopped.

Figure 8 shows the time history of the predicted pin kinetic energy. A continual increase in kinetic energy to a maximum value of near $4.4\ J$ occurs until the

effects of friction start to dominate. The frictional force continues to perform work on the pin until the pin's kinetic energy decreases to near $3.6\ J$ at the time of contact of the crush cap with the end cap, t_c. The strain-rate force of the cap, F_v, and the frictional force, F_f, dissipate the final portion of pin's kinetic energy.

Figure 9 shows the time history of the various forces (F_p, F_f, F_e, F_v) which influence the pin motion, and Fig. 10 shows the time history of the pyrotechnic shock force F_{ps}. It is seen that F_{ps} is negative (to the right) at early time so as to balance the pressure force, F_p which pushes against the surrounding structure to the left. After the cup strikes the end cap, forces which tend to push the surrounding structure to the right dominate to the extent that F_{ps} must be positive (to the left) to hold the structure stationary. The amplitude of F_{ps} is over $2\ kN$. At long time F_{ps} relaxes to near zero, as the pin comes nearly to rest in a position in which F_p approaches F_e, and both F_v and F_f, being velocity dependent, relax to near
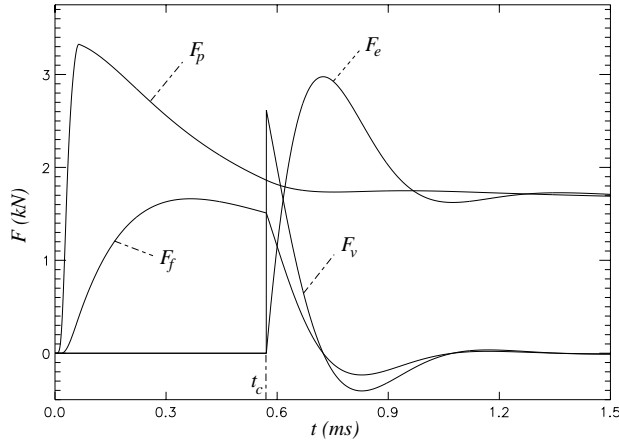
9

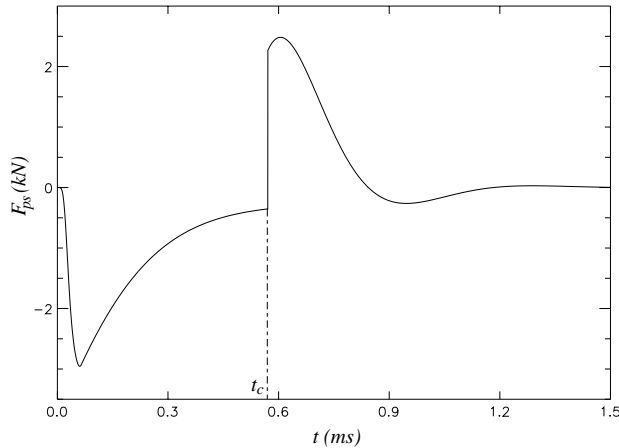Figure 9: Forces acting on the pin during its stroke.

Figure 10: Pyrotechnic shock force, F_{ps}, necessary to hold surrounding structure stationary.

zero. Neither F_{ps} nor the pin velocity have relaxed exactly to zero in these simulations as the calculations have not been carried out to a point where the subsystems are in thermal equilibrium with the surroundings. There is a long time scale thermal equilibration process still occurring, during which mechanical equilibrium is maintained, in which the pressure drops slowly as the gases cool, giving rise to the elastic force relaxing so as to match the pressure force.

Conclusions

The model presented in this paper is successful in predicting the dynamic events associated with the operation of an NSI driven pin puller. In addition to tracking the interactions between the reactant and product subsystems, the model also accounts for multiple pyrotechnic grains, variable burn surface area, combustion product mass flow rates through the port,

and crush of the energy absorbing cap. The model of the crush of the energy absorbing cap presented in this paper represents a starting point for quantifying the pyrotechnic shock associated with an NSI device, which may have been a contributing factor in the failure of the Mars Observer. A natural continuation of this research would be a parametric study which sought ways to reduce peak shock amplitudes and impulse while maintaining piston stroke time.

References

[1]Bement, L. J., Multhaup, H. A., and Schimmel, M. L., "HALOE Gimbal Pyrotechnic Pin Puller Failure Investigation, Redesign, and Qualification," NASA Langley Research Center, Report, Hampton, VA, 1991.

[2]Gonthier, K. A., and Powers, J. M., "Formulation, Predictions, and Sensitivity Analysis of a Pyrotechnically Actuated Pin Puller Model," *Journal of Propulsion and Power*, Vol. 10, No. 4, 1994, pp. 501-507.

[3]Gonthier, K. A., and Powers, J. M., "Choked Flow Effects in the NSI Driven Pin Puller," Second NASA Aerospace Pyrotechnic Systems Workshop, February 1994.

[4]David, L., "Observing a Failure," *Aerospace America*, Vol. 32, No. 6, 1994, pp. 28-33.

[5]Kuo, J. H., and Goldstein, S., "Dynamic Analysis of NASA Standard Initiator Driven Pin Puller," AIAA 93-2066, June 1993.

[6]Gordon, S., and McBride, B. J., "Computer Program for Calculation of Complex Chemical Equilibrium Compositions, Rocket Performance, Incident and Reflected Shocks, and Chapman-Jouguet Detonations," NASA Lewis Research Center, SP-273, Cleveland, OH, 1976.

[7]Fox, R. W., and McDonald, A. T., *Introduction to Fluid Mechanics,* 3rd *ed.*, John Wiley and Sons, Inc. New York, 1985.

[8]Bement, L. J., private communication, NASA Langley Research Center, Hampton, VA, 1992.

[9]Baglini, J., private communication, OEA Inc., Denver, 1994.